LRP 447/91 December 1991

PARASITIC OSCILLATION IN AND SUPPRESSION OF A GYRO BW MODE IN A LOW-Q 8GHz GYROTRON

P. Muggli, M.Q. Tran, T.M. Tran

submitted for publication to
IEEE Transactions on Plasma Science

Parasitic oscillation in and suppression of a gyro BW mode in a low-Q 8 GHz gyrotron

P. Muggli, M.Q. Tran and T.M. Tran

Centre de Recherches en Physique des Plasmas,

Association Euratom-Confédération Suisse,

Ecole Polytechnique Fédérale de Lausanne,

21, Av. des Bains, CH-1007 Lausanne,

Switzerland

Abstract

The parasitic oscillation of the TE^{o}_{21} gyrotron Backward Wave (gyro BW) mode is observed in a low-Q, 8 GHz TE^{o}_{011} gyrotron. Although at low power (P_{BW}<5 kW), the oscillation of the gyro BW mode, simultaneously with the gyrotron mode, results in a maximum TE^{o}_{011} mode efficiency of less than 0.25. The parasitic oscillation is suppressed by operating the gyrotron with a negative magnetic field gradient along the electron beam, which allows the maximum efficiency to reach 0.40 and the output power to be multiplied by a factor varying from 1.4 to 1.7. The optimum efficiency curve of the TE^{o}_{011} mode indicates that the low-Q cavity behaves as a much higher Q_{diff} cavity. Too large magnetic field gradient and α values favour the TE^{o}_{012} longitudinal mode, which oscillates in place of the TE^{o}_{011} mode and limits its maximum output power. This competitive process is responsible for the high-Q like behavior of the optimum efficiency curve.

I. Introduction

The gyrotron is a powerful microwave source in which an electron beam, operating under the cyclotron resonance condition, excites one of the cavity eigenmodes. Power levels above one megawatt have been experimentally obtained with efficiencies higher than 0.30 both at low (8 GHz) (1) and high (140 GHz) (2,3) frequencies. The gyrotron output power is mainly limited by technological constraints such as the maximum allowable ohmic losses on the cavity wall, energy deposition of the spent electron beam on the collector and microwave power absorption in the dielectric output window (4). Measured efficiencies are usually lower than computed efficiencies. This discrepancy is mainly attributed to space charge effects, in the gun and magnetic field compression region, which increase the beam velocity dispersions and prevent the beam from reaching a high velocity ratio ($\alpha=<v_\perp>/<v_\parallel>$) at high current (3,5). Another mechanism that could contribute to this discrepancy is the oscillation, at relatively low power (as compared to the gyrotron mode) and simultaneously with the gyrotron mode, of gyrotron Backward Wave (gyro BW) modes corresponding to absolute instabilities of the system. A gyro BW mode has been observed in two of the megawatt tubes (1,2). Its oscillation was considered as the cause of the degradation of the gyrotron efficiency in one of these experiments (6). The optimum gyrotron interaction length, when considering a gaussian longitudinal electric field profile in the cavity, is of six to seven vacuum wavelengths of the operating mode (7). The minimum starting length for gyro BW modes (L_{start}) is of less than five vacuum wavelengths for an electron beam typical for gyrotrons ($U_{cath}>60$ kV, $I_b>4$ A, $\alpha\cong2.0$) (8). These two lengths being comparable, the oscillation of gyro BW modes is very likely in high power, low-Q cavity gyrotrons.

In our low-Q, TE^{o}_{011}(Q_{diff}=160), 8 GHz gyrotron experiment the oscillation of the TE^{o}_{21} gyro BW mode is observed (9). This parasitic mode oscillates simultaneously with the gyrotron mode and thus prevents its efficiency from reaching more than 0.25. The oscillation of the gyro BW mode can be suppressed by operating the gyrotron with a negative magnetic field (B-field) gradient along the electron beam flow. Under these conditions, the achieved efficiency of the TE^{o}_{011} mode is 0.40 and the optimum output power is multiplied by a factor of 1.4 to 1.7, depending on the beam current. In our experiment, the output power and efficiency are limited by the oscillation of the TE^{o}_{012} longitudinal mode which replaces the TE^{o}_{011} mode at high B-field gradient.

This paper is organized as follows. Section II gives a description of the experimental set-up and diagnostics. The characteristics of the TE^{o}_{21} gyro BW mode are given in section III. The influence of this parasitic mode on the gyrotron mode and the results of its suppression along with the TE^{o}_{011} power optimization are given in section IV. Conclusions are presented in section V.

II. Experimental set-up

The gyrotron cavity is characterized by the very low diffractive quality factor of the TE^{o}_{011} mode : Q_{diff}=160 at 8.005 GHz. This low value is chosen to obtain a maximum electronic efficiency ($\eta_{el} \cong 0.5$) at a beam current I_b of about 10 A; the maximum that the high voltage regulator power supply can deliver at a cathode voltage U_{cath} of 75 kV. The TE^{o}_{011} mode has been chosen because dispersion curves indicate that there is no nearby competiting gyrotron mode (Fig. 1), and because non-linear calculations show that a power in excess of 400 kW can, in principle, be obtained with a 10 A beam current (α=1.75). At 8 GHz and up to 20 A, the beam charge

density is low and allows the use of volume modes. The length of the cavity is of about 4.5 vacuum wavelengths. The electron gun (a diode Magnetron Injection Gun) has been designed with the EGUN code (10) to produce at the cavity entrance an annular beam of radius 1.1 cm with a velocity ratio $\alpha=<v_\perp>/<v_\parallel>$ of 1.75 and with low velocity dispersions : $(\Delta v_\perp/<v_\perp>)\leq 0.02$ and $(\Delta v_\parallel/<v_\parallel>)\leq 0.05$ for $I_b\leq 10$ A. However, α values up to 2.4 can also be obtained experimentally by increasing the adiabatic magnetic compression ratio (9). The collector and output waveguide corresponds to a C18 overmoded waveguide ($f_{cut\text{-}off}(TE^o_{01})=3.19$ GHz). The output window is a single alumina disc matched to the TE^o_{01} mode around 8.0 GHz.

A wavenumber spectrometer (11) is used to obtain the mode content of the outcoming radiation. It can be calibrated for the modes of interest (TE^o_{01q} q=1,2 and TE^o_{21}) against an octanol calorimeter by choosing the B-field such that the cavity oscillates in only one of these modes (Fig. 2). In particular, in this experiment it is possible to measure during two consecutive microwave pulses the output powers of both the TE^o_{01} and TE^o_{21} modes when they oscillate simultaneously, with relative measurement errors of ±5% and ±25%, respectively. The large error on the TE^o_{21} mode is due to the dependence of the wavenumber spectrometer coupling factor as a function of the gyro BW oscillation frequency which varies between 6.8 and 7.3 GHz with the experimental parameters α, I_b, and magnetic field B_0. Estimations of the oscillation frequencies are given by frequency discriminators and rectangular waveguide filters. A precise measurement (±300 MHz) is obtained with a spectrum analyzer during a 15 ms microwave pulse.

III. Characteristics of the TE^{o}_{21} gyro BW mode

Figure 2 shows the experimental mode map of the gyrotron for U_{cath}=75 kV and $\alpha_{EGUN}\cong$1.75. It is characterized by the oscillation over most of the tube operating domain of the TE^{o}_{21} gyro BW mode with a frequency ranging from 6.8 to 7.3 GHz. This mode of oscillation corresponds to the interaction between the backward component of the TE^{o}_{21} waveguide mode in the gyrotron cavity and the first harmonic of the electron cyclotron frequency $\Omega_{c0}=eB_0/m_0$:

$$\omega_{BW} = \frac{\Omega_{c0}}{\gamma} - |k_{\parallel}| v_{\parallel} \qquad (1)$$

where γ is the electron relativistic factor and $k_{\parallel}$ is the component of the wavenumber ($k=\omega/c$) parallel to the waveguide axis. Such an interaction involving waves with oppositely directed group velocities (Fig. 1) in a system where the interaction length L_i is finite, can result in an absolute instability above a certain beam current threshold. The amplitude of the oscillation can then grow exponentially both in space and time, without the need of an external cavity feedback. The experimental oscillation characteristics of the TE^{o}_{21} mode (frequency and output power) are obtained at low B-field (B_0<3.095 kG), where the output is single-moded.

The nonlinear wave-particle interaction is described by a numerical simulation which solves self-consistently the slow time-scale particle and wave equations. These calculations show that the interaction length L_i in the gyrotron cavity is about 24 cm ($L_i\cong5.6\lambda_{vacuum}$, cf. Fig. 7.a). In the experiment the TE^{o}_{21} mode, identified by its wavenumber spectrum and oscillation frequency, needs the full gyrotron cavity length to oscillate. The mode starts at the cavity output ($|E_{BW}(z=L_i)|\cong0$) and travels backward to the cavity input. It

is reflected by the cut-off section, which prevents the waves from reaching the electron gun, and travels forward to the matched load without interacting with the beam ($\omega_{BW} << \omega_{FW} = \Omega_{c0}/\gamma + k_{||} v_{||}$). The single disc gyrotron window which is matched to the TE^{o}_{01} mode at 8.0 GHz, exhibits a power reflection coefficient ρ from 0.13 to 0.32 for the TE^{o}_{21} in the frequency range of 6.8 to 7.3 GHz. The window mismatch and the long line effect explain the observed discontinuous dependance of the gyro BW frequency as a function of the experimental parameters α, B_0, I_b (Fig. 3). The frequency gap Δf_{line} and the bandwidth $\Delta f_{Q_{line}}$ of the characteristic stopband-passband structure are given by :

$$\Delta f_{line} = \frac{\omega}{2\, k_{||}\, L_{line}} \tag{2}$$

$$\Delta f_{Q_{line}} = \frac{\omega}{2\pi\, Q_{line}} \tag{3}$$

where Q_{line} is the quality factor of the cavity of length L_{line} formed by the gyrotron cavity, the collector and the mismatched window ($L_{line} \cong 33\lambda_{||}$ at 7 GHz). It is given by (12) :

$$Q_{line} = \frac{2\,\omega\, k\, L_{line}}{c\, k_{||}\, \ln(\rho)}. \tag{4}$$

The measured values are $\Delta f_{line} \cong 60$ MHz and $\Delta f_{Q_{line}} \cong 18$-25 MHz, in very good agreement with the values given by (2) to (4), $\Delta f_{line} \cong 67$ MHz, and $\Delta f_{Q_{line}} \cong 18$-29 MHz for $\rho = 0.32$-0.13. The window matching to the TE^{o}_{21} mode can be improved ($\rho = 0.0$-0.15) (Fig. 3), while keeping the matching to the TE^{o}_{01} mode around 8.0 GHz (corresponding to the TE^{o}_{011} cavity mode) by adding a second identical alumina disc at a distance of 3.9 cm from the first one. This method renders the frequency dependance with respect to changes of

the experimental parameters almost continuous, and diminishes the gyro BW output power by a factor of approximately two (cf. Fig. 11).

Although with the matched window system the oscillation frequency behaves smoothly, for example as a function of the beam current, the output power does not (Fig. 4). This somewhat erratic behavior is probably due to the interference, in the gyrotron cavity, of the backward growing wave and the wave reflected by the imperfectly matched window. The effect of this interference may be more pronounced since the interaction length is very close to the minimum starting length ($L_{start} \cong 5\lambda_{vacuum}$).

The measured output power is less than 13.0±3.25 kW for beam currents up to 8 A and α_{EGUN} values up to 2.2; whereas, calculations for a cold electron beam indicate that the output power should be 48 kW for I_b=8 A, α=1.75 and B_0=2.97 kG. As the interaction of gyro BW modes depends on the beam parallel velocity (cf. (1)), their oscillation frequency and output power are very sensitive functions of the beam velocity dispersions (Fig. 5). A comparison between α values given by the EGUN code and values deduced from the TE^{o}_{21} mode oscillation frequency (9) seems to indicate that the actual velocity dispersions are larger than given by the EGUN code : $(\Delta v_\perp / \langle v_\perp \rangle) \cong 0.04$ and $(\Delta v_\parallel / \langle v_\parallel \rangle) \cong 0.12$ for I_b=5 A and α=1.75. Such large dispersion values could account for the low measured output powers.

The TE^{o}_{21} gyro BW mode has not been observed with the other gyrotron prototypes (13,14), which had higher Q_{diff} values for the TE^{o}_{011} mode. It has been observed with the Q_{diff}=225 cavity in presence of power reflection only (14). The Q_{diff}=160 cavity was obtained from the Q_{diff}=225 cavity by slightly changing the opening angle of the straight section (0.1° to 0.2°). The length of the two cavities is thus the same and all the other parts (gun, collector, window) are identical for the two tubes. The appearance of the gyro BW mode is not understood; however, because the gyrotron

cavity length is close to the minimum starting length, minor changes to the tube geometry may make the difference between whether the mode oscillates or not.

The forward component of the TE^{o}_{21} mode ($\omega_{FW}=\Omega_{c0}/\gamma+|k_{||}|v_{||}$), corresponding to the convective instability used in the gyrotron travelling wave amplifiers (gyro TWA), is also observed at low α ($\alpha_{EGUN}<1.3$) and high magnetic field ($B_0>3.22$ kG) values with a frequency ranging from 9.58 to 10.50 GHz. The oscillation of this mode is possible only because of the large amplitude of the power reflection coefficient of the gyrotron window (ρ=0.19-0.58) for the TE^{o}_{21} mode in this frequency range.

IV. Suppression of the TE^{o}_{21} gyro BW mode

Non-self-consistent (NSC) and self-consistent (SC) calculations show that, with the $Q_{diff}(TE^{o}_{011})$=160 cavity, the maximum electronic efficiency ($\eta_{el}\cong$0.5 with α=1.75 and U_{cath}=75 kV) should be obtained around 11 A and 7 A for the two calculation methods, respectively. Experimentally, for each beam current the TE^{o}_{011} mode output power is optimized with respect to the magnetic field B_0 and with respect to the beam parameters through the magnetic compression. In principle, the output power increases with α as long as the magnetic field B_0 is adjusted to maintain the optimum detuning (7). However, as α increases the beam velocity dispersions increase, and as a result the output power decreases. Figure 6 shows the results of the optimization with a flat B-field profile along the cavity. At all beam currents, the TE^{o}_{21} gyro BW mode oscillates at low power ($P_{BW}<5$ kW), simultaneously with the TE^{o}_{011} gyrotron mode. As a consequence, the gyrotron efficiency remains below 0.25 for beam currents between 2 and 9 A. The gyro BW mode perturbs the gyrotron mode through two mechanisms, both of them

related to the large electric field amplitude of the TE^{o}_{21} mode near the cavity input (Fig. 7.a). Figure 7.b shows that particles entering the cavity absorb more energy from the TE^{o}_{21} mode than from the TE^{o}_{011} mode. When the two modes oscillate simultaneously, the TE^{o}_{21} mode around 7 GHz has a strong mixing effect on the phase-bunching of the particles with respect to the TE^{o}_{011} mode at 8 GHz. The first mechanism is thus the perturbation of the electron phase bunching with respect to the gyrotron mode. The second mechanism is the introduction of large beam parameters dispersions. As an example, for the TE^{o}_{21} mode with a single mode efficiency of only 0.055 (Fig. 7.c), the perpendicular velocity dispersion $\Delta v_\perp/\langle v_\perp\rangle|_{out}$, defined using the standard deviation $\Delta v_\perp$ and the average $\langle v_\perp\rangle$ of the electrons' perpendicular velocity at the output of the cavity, is as large as 0.15. For the same parameters, the gyrotron mode reaches a single mode efficiency of 0.31 but the $\Delta v_\perp/\langle v_\perp\rangle|_{out}$ it introduces is only 0.25 (Fig. 7.d). When entering the cavity, electrons experience a large TE^{o}_{21} electric field amplitude and $\Delta v_\perp/\langle v_\perp\rangle$ increases very quickly with z (Fig. 7.c) while the electric field amplitude increases adiabatically for the TE^{o}_{011} mode. Figure 8 shows the influence of velocity dispersions on the output power of the gyrotron mode. For these calculations, we have considered a low charge density electron beam ($\Delta\gamma/\langle\gamma\rangle\cong 0$), i.e. the velocity dispersions are related by :

$$\frac{\Delta v_\perp}{\langle v_\perp\rangle} = \frac{1}{\alpha^2}\frac{\Delta v_\parallel}{\langle v_\parallel\rangle} \qquad (5)$$

The dispersions introduced along the electron beam by the oscillation of the gyro BW mode do not satisfy this relation. Note that the numerical results presented in this paper are obtained separately for the two modes of oscillation (single-mode calculations). To describe the mutual interaction between these two modes, a multi-mode calculation would be necessary.

The TE^{o}_{21} gyro BW mode parasitic oscillation can be suppressed by operating the gyrotron with a negative B-field gradient along the electron beam flow. In the experiment, six coils are used to generate a linear variation of the B-field in the cavity region of the form :

$$B_0(z) = B_0\left(1 + (z - z_0)\frac{\delta B_0}{L_B B_0}\right) = B_0\left(1 + (z - z_0)\, g\right) \qquad (6)$$

where z_0 is the coordinate of a point located at the middle of the straight section of the cavity where the B-field value is B_0, and around which the B-field profile is varied, and δB_0 is the variation of the B-field over L_B, the length over which B_0 is constant at ±1% in the flat profile case ($g=0$, $L_B \cong 0.18$ m). The effect of the B-field gradients on both the TE^{o}_{21} and TE^{o}_{011} modes can be computed and measured experimentally. In both cases, results show that negative B-field gradients ($g<0$) tend to strongly decrease the gyro BW mode output power, and, for a given value of α at the cavity input, tend to slightly increase the gyrotron mode output power (Figs. 9,10,11). The experimental g-values necessary to suppress the gyro BW mode ($g<-0.2$ in Fig. 11) when it oscillates in single mode ($B_0<3.095$ kG) are in very good agreement with the computed values (Fig. 9). The measured TE^{o}_{011} mode output power increase caused caused by this range of g-values is also in very good agreement with the computed one (Fig. 10). The single-mode TE^{o}_{011} oscillation can be obtained and optimized including B-field gradients. The results are shown in Fig. 12. The TE^{o}_{21} parasitic mode is completely suppressed and, depending on the beam current, the TE^{o}_{011} mode output power is multiplied by a factor 1.4 to 1.7 with respect to the optimization with a flat B-field profile. The maximum efficiency is 0.402. The observed power increase is monotonic with decreasing g; however, in our experiment, it is limited by the oscillation of the TE^{o}_{012} mode at excessively large gradient

values in place of the TE^{o}_{011} mode. The TE^{o}_{012} mode output power is lower than the TE^{o}_{011} power for comparable experimental parameters. The window system matched to the gyro BW mode, described in the previous section and which allows its output power to be diminished by a factor of about two, is not used during the gyrotron mode output power optimization. Although this two windows system is matched for the TE^{o}_{01} mode at 8.0 GHz (corresponding to the TE^{o}_{011} resonant mode of the cavity), its reflection coefficient around 8.1 GHz (corresponding to the TE^{o}_{012} resonant mode of the cavity) is sufficient to often induce the oscillation of the the TE^{o}_{012} cavity mode in place of the TE^{o}_{011}, even with g=0.

The electronic efficiency curves, computed self-consistently and non-self-consistently for α=1.75, show that self-consistent effects (i.e. modification of the longitudinal electric field profile of the resonant mode by the beam-wave coupling) have a strong influence on the efficiency achievable with the Q_{diff}=160 cavity ($I_b(\eta_{max\ SC})\cong 5$ A<$I_b(\eta_{max\ NSC})\cong 11$ A). The maximum experimental efficiency (η=0.402 with α_{EGUN}=2.15, $\Delta v_\perp/\langle v_\perp\rangle_{EGUN}$=0.014, $\Delta v_\parallel/\langle v_\parallel\rangle_{EGUN}$=0.063, $\Delta\gamma/\langle\gamma\rangle_{EGUN}=2\cdot10^{-4}$) is obtained at I_b=3 A (Fig. 13). The high-Q like behavior of the cavity, suggested by the shift toward low current of the experimental efficiency curve obtained with g<0 (Fig. 13), is attributed to the high α_{EGUN}-values for which the optimum output power is achieved at low current (I_b<5 A). At high beam current (I_b>5 A), the maximum output power is limited by the oscillation at low power of the TE^{o}_{012} mode in place of the TE^{o}_{011} mode, when α_{EGUN} and negative-g values become too large (α_{EGUN}>2.0 and g<-0.286) (Fig. 14). Moreover, the computed SC effect of negative g-values on η_{el} is to cause it to increase at low beam current and to decrease at high beam current (Fig. 13). The shape of the experimental efficiency curve is well reproduced by SC calculations using the experimental values of g and α (α_{EGUN} given on Fig. 14) and a cold electron beam. The

difference between these two efficiencies ($0.053<(\eta_{SC}-\eta_{exp})<0.083$) is explained by the beam velocity dispersions.

It is not possible to determine experimentally which fraction of the power increase can be attributed to the suppression of the parasitic mode and which fraction can be attributed to the effect of B-field gradients on the gyrotron mode. But, there are indications that most of the power increase has to be attributed to the suppression of the gyro BW mode. Firstly, numerical results on the TE^{o}_{011} mode show that, while keeping the value of α constant at the cavity input, the values of g used in the experiment do not increase the output power by more than 25% with respect to the g=0 case (Fig. 9). The observed 40 to 70% of power increase can therefore not be attributed only to the presence of B-field gradients. Moreover, the measured effect of negative g-values on the TE^{o}_{011} single-mode output power, taking into account the actual α-value at the cavity input for a given B_0, is lower or equal to the computed one (Fig. 10). Finally, the values of α_{EGUN} (and thus the average α-value along the interaction region) for which the optimum power is obtained when g<0 are usually smaller than when g=0 (Fig. 14). Thus the observed power increase is not due to an increase of the perpendicular kinetic energy of the electrons, but to an increase of the perpendicular efficiency $\eta_{\perp}$, defined by :

$$\eta_{\perp} = \frac{2}{\beta_{\perp 0}}(1 - \langle\gamma\rangle/\gamma_0) = \frac{2\gamma_0}{(1+\gamma_0)}\frac{(1+\alpha^2)}{\alpha^2}\eta_{el} \qquad (7)$$

where $\eta_{el} = (\gamma_0 - \langle\gamma\rangle)/(\gamma_0 - 1)$, and γ_0, $\beta_{\perp 0}$ and α are the values at the input of the cavity (z=0). The perpendicular efficiency is from 1.5 to 1.9 times larger with g<0 than with g=0.

V. Conclusion

The oscillation at low power (P_{BW}<13 kW) of the backward travelling component of the TE^{o}_{21} mode is observed in a low-Q, 8 GHz, TE^{o}_{011} gyrotron. Its oscillation, simultaneously with the TE^{o}_{011} mode, prevents the gyrotron efficiency from reaching more than 0.25, through both the perturbation of the electrons phase bunching with respect to the gyrotron mode, and the introduction of large perpendicular velocity dispersion along the second half of the cavity. The oscillation of the gyro BW mode is suppressed by operating the gyrotron with a negative magnetic field gradient along the electron beam flow. Thanks to this suppression, the gyrotron efficiency reaches a maximum of 0.402 at a beam current of 3 A. The experimental results show that the optimum efficiency at low current (I_b<5 A) and with g<0 is obtained at high α values (α_{EGUN}>2.0). At higher beam current (I_b>5 A), the value of α must be decreased to maintain the oscillation in the TE^{o}_{011} mode, since both large values of α and of the negative B-field gradient g favour the oscillation of the TE^{o}_{012} mode at low power in place of the TE^{o}_{011}. It is the oscillation of the TE^{o}_{012} mode which limits the main mode output power and gives a high-Q like behavior to the optimum efficiency curve.

Negative B-field gradients (g<0) provide a general means of suppressing the oscillation of parasitic gyro BW modes. They increase the gyrotron mode output power at low beam current, but lead to the oscillation of the q=2 component in place of the TE^{o}_{mpq} q=1 mode which limits their favorable influence.

Acknowledgment

We would like to acknowledge the technical support of the Department of EKR of ABB-Infocom SA. We would like to thank Dr. T. Goodman for a careful reading of the manuscript. This work was partially supported by the Fonds National de la Recherche Scientifique.

References

(1) P. Garin, G. Mourier, J.M. Krieg and A. Dubrovin, "Extensive experimental results on a 1 MW, 8 GHz gyrotron and the transmission line", Conference digest of the 15th Int. Conf. on Infrared and Millimeter Waves, Orlando, 10-14 Dec., Vol SPIE 1514, pp. 768-770, (1990).

(2) K.Y. Xu, K.E Kreisher, W.C. Guss, T.L. Grimm and R.J. Temkin, "Efficient operation of a megawatt gyrotron", Conference digest of the 15th Int. Conf. on Infrared and Millimeter Waves, Lake Buena Vista, 14-18 Dec., Vol SPIE 1514, pp. 324-326, (1990).

(3) K. Felch, C. Hess, H. Huey, E. Jongewaard, H. Jory, J. Nielson, R. Pendleton and M. Tsiruluikov, "Recent long-pulse and high-average-power tests on a 140 GHz gyrotron", Conference digest of the 15th Int. Conf. on Infrared and Millimeter Waves, Lake Buena Vista, 14-18 Dec., Vol SPIE 1514, pp. 315-317, (1990).

(4) K. Felch, H. Huey and H. Jory, "Gyrotrons for ECH applications", J. Fusion Ener. **9**(1), pp. 59-75, (1990).

(5) W.C. Guss, T.L. Grimm, K.E. Kreisher, J.T. Pelevoy and R.J. Temkin, "Velocity ratio measurements of a gyrotron electron beam", J. Appl. Phys. **69**(7), pp. 3789-3795, (1991).

(6) T.M Antonsen Jr., S.Y. Cai, G. Saraph, B. Levush, W.C. Guss, M. Basten, K.E. Kreisher and R.J. Temkin, "Excitation of parasitic waves in high power gyrotrons : theory and experiment", Conference digest of the 16th Int. Conf. on Infrared and Millimeter Waves, Lausanne, 26-30 Aug., Vol SPIE 1576, pp. 51-52, (1991).

(7) B.G. Danly and R.J Temkin, "Generalized nonlinear harmonic gyrotron theory", Phys. Fluids **29**(2), pp. 561-567, (1986).

(8) W.C. Guss, K.E. Kreisher, and R.J. Temkin, "Operation of a 140 GHz tunable backward wave gyrotron oscillator", Conference digest of the 13th Int. Conf. on Infrared and Millimeter Waves, Hawaii 5-9 December, Vol. SPIE 1039, pp. 369-370, (1988).

(9) P. Muggli, M.Q. Tran and T.M. Tran, "Velocity ratio measurement using the frequency of the gyro backward wave", Phys. Fluids B-**3**(6), pp. 1315-1318, (1991).

(10) W.B. Hermannsfeldt, Electron trajectory program, SLAC 226, Stanford linear accelerator center, Stanford CA 94305, November 1979, (1979).

(11) W. Kasparek and G.A. Müller, "The wavenumber spectrometer-an alternative to the directional coupler for multimode analysis in oversized waveguides", Int. J. Electronics **64**(1), pp. 5-20, (1988).

(12) S.N. Vlasov, G.M. Zhislin, I.M. Orlova, M.I. Peletin and G.G. Rogocheva, "Irregular waveguides as open resonators" Radiophys. Quant. Electron. **12**(8), pp. 972-978, (1969).

(13) H.-G. Mathews, G. Agosti, K. Holm, D. Kuse, P. Muggli, M.Q. Tran, S. Alberti, A. Perrenoud and T.M. Tran, "A high power gyrotron oscillator at 8 GHz", Conference digest of the 12th Int. Conf. on Infrared and Millimeter Waves, Lake Buena Vista, 14-18 Dec., pp. 383-384, (1987).

(14) P. Muggli, M.Q. Tran, T.M. Tran, H.-G. Mathews, G. Agosti, S. Alberti and A. Perrenoud, "Effect of power reflection on the operation of a low-Q 8 GHz gyrotron", IEEE Trans. on Microwave Theory and Tech. **MTT-38**(9), pp. 1345-1351, (1990).

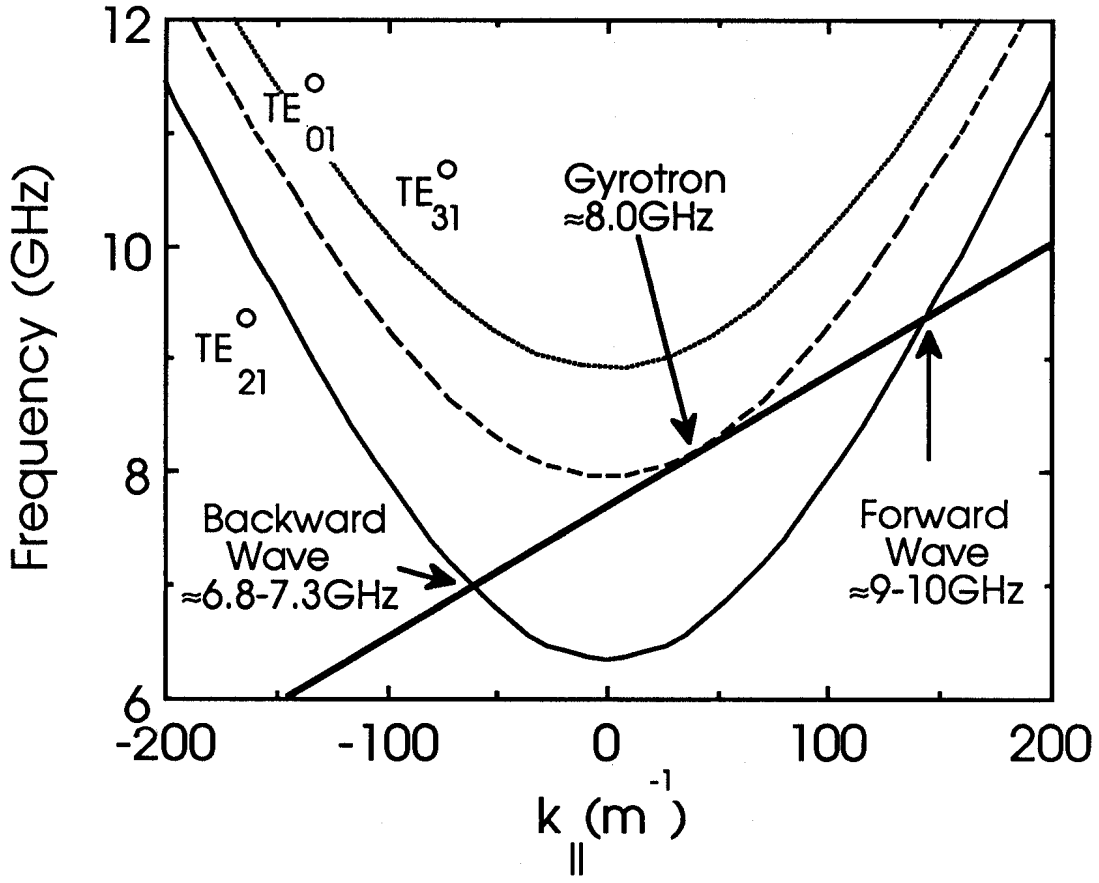

Figure 1

Dispersion curves for the first harmonic electron cyclotron beam mode ($\omega=\Omega_{c0}/\gamma+k_{||}v_{||}$, thick line) and for the TE^{o}_{01} (dashed line), TE^{o}_{21} (continuous line) and TE^{o}_{31} (dotted line) waveguide modes ($\omega=(k^2_{||}+k^2_{\perp})^{1/2}c$). Beam-wave interaction occurs for ω and $k_{||}$ corresponding to the dispersion curves intersections. In this case the three possible types of interaction are the TE^{o}_{01} gyrotron mode ($\omega\cong\Omega_{c0}/\gamma$, $k_{||}\cong 0$), the backward ($\omega_{BW}\cong\Omega_{c0}/\gamma-|k_{||}|v_{||}$, $k_{||}<0$, gyro BW) and the forward ($\omega_{FW}\cong\Omega_{c0}/\gamma+|k_{||}|v_{||}$, $k_{||}>0$, gyro TW) TE^{o}_{21} mode components.

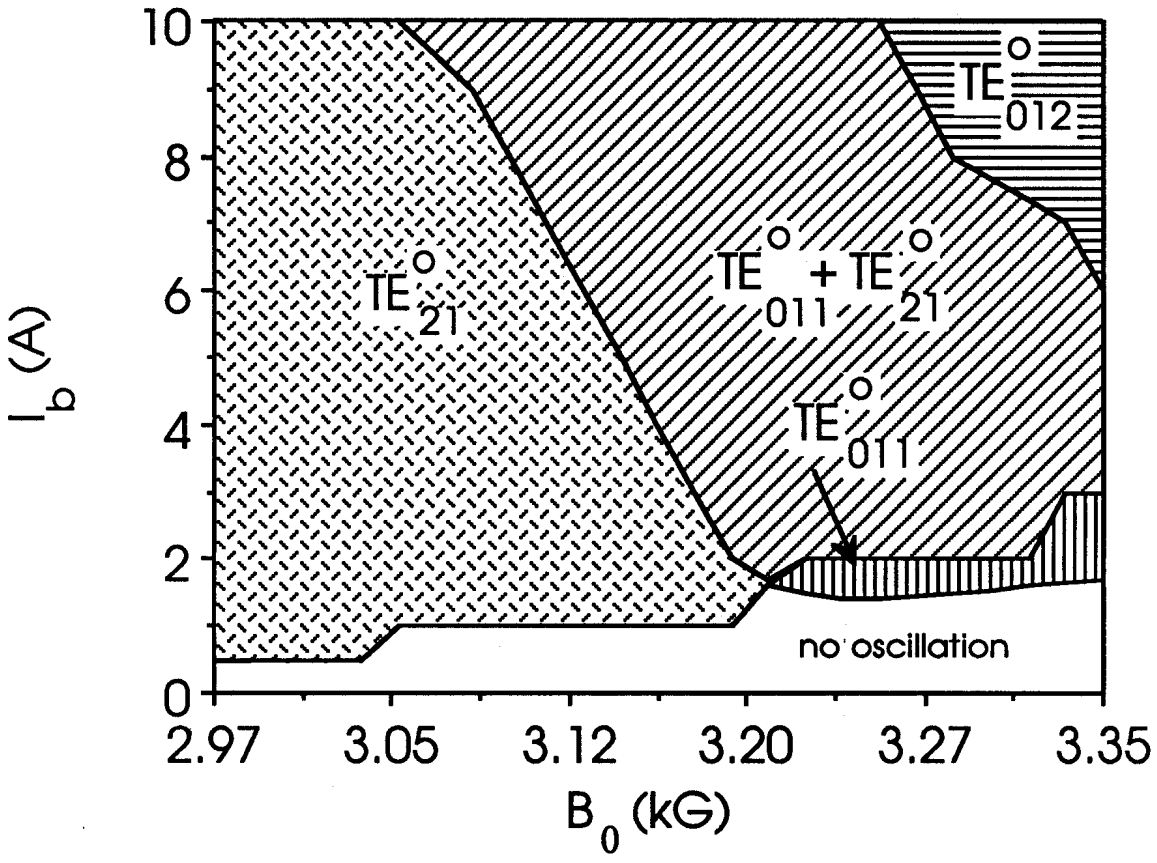

Figure 2

Experimental mode map for the cavity with $Q_{diff}(TE^o_{011})$=160 at 8.005 GHz and for U_{cath}=75 kV and $\alpha_{EGUN} \cong 1.75$. The TE^o_{01q} q=1,2 and TE^o_{21} modes are identified by their oscillation frequency : 8.000 to 8.080 GHz for the q=1 and 8.080 to 8.125 GHz for the q=2 gyrotron mode components and 6.8 to 7.3 GHz for the gyro BW mode, and by their characteristic TE^o_{01} and TE^o_{21} wavenumber spectrum in the C18 output waveguide.

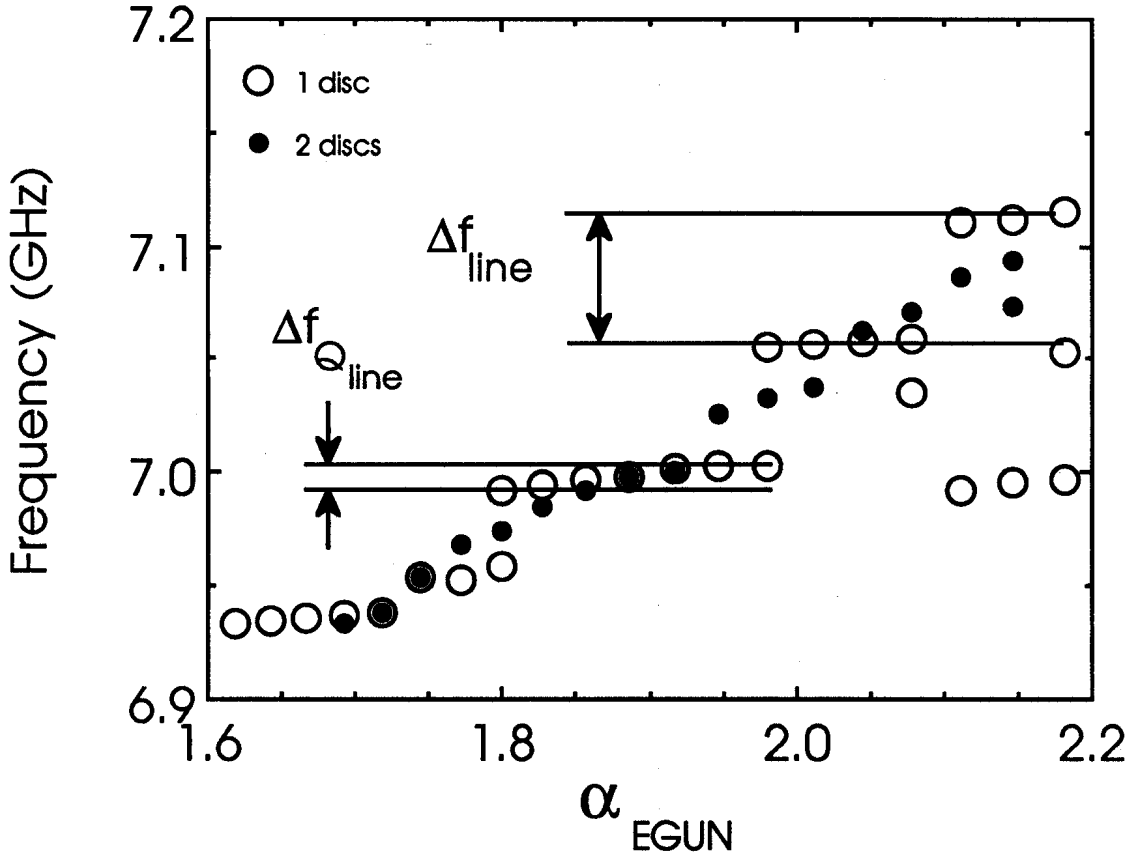

Figure 3

Oscillation frequency of the TE^{o}_{21} gyro BW mode measured as a function of the experimental beam velocity ratio α_{EGUN}, with a single alumina disc window (ρ=0.13-0.32 between 6.8 and 7.3 GHz, open circles), and with a "matched" window system (ρ=0.0-0.15, filled circles) consisting of two identical alumina discs separated by 3.9 cm. The value of Δf_{line} and $\Delta f_{Q_{line}}$ obtained experimentally (60 MHz and 18-25 MHz respectively) are in good agreement with the values obtained from (2) to (4) with a line length of $33\lambda_{||}$ and ρ=0.32-0.13 at 7.0 GHz (67 MHz and 18-29 MHz, respectively). U_{cath}=75 kV, I_b=4 A, B_0=3.033 kG.

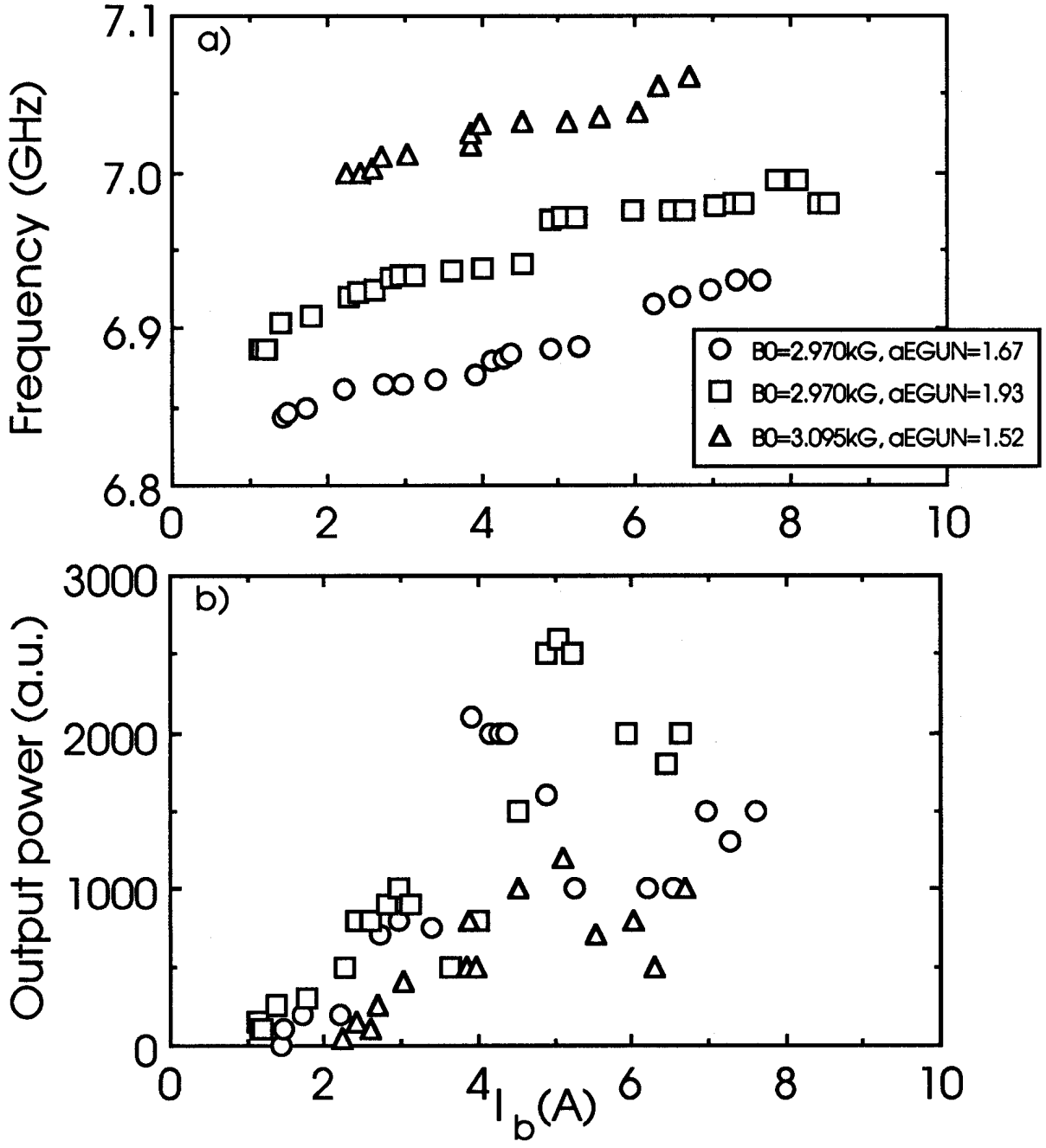

Figure 4

Measured oscillation frequency a) and output power b) of the TE_{21}^{o} gyro BW mode as function of the beam current I_b. The oscillation frequency has a continuous dependance on I_b, whereas the output power behaves non-smoothly. U_{cath}=75 kV, B_0 and α_{EGUN} are respectively : 2.97 kG and 1.67 (circles), 2.97 kG and 1.93 (squares), 3.095 kG and 1.52 (triangles).

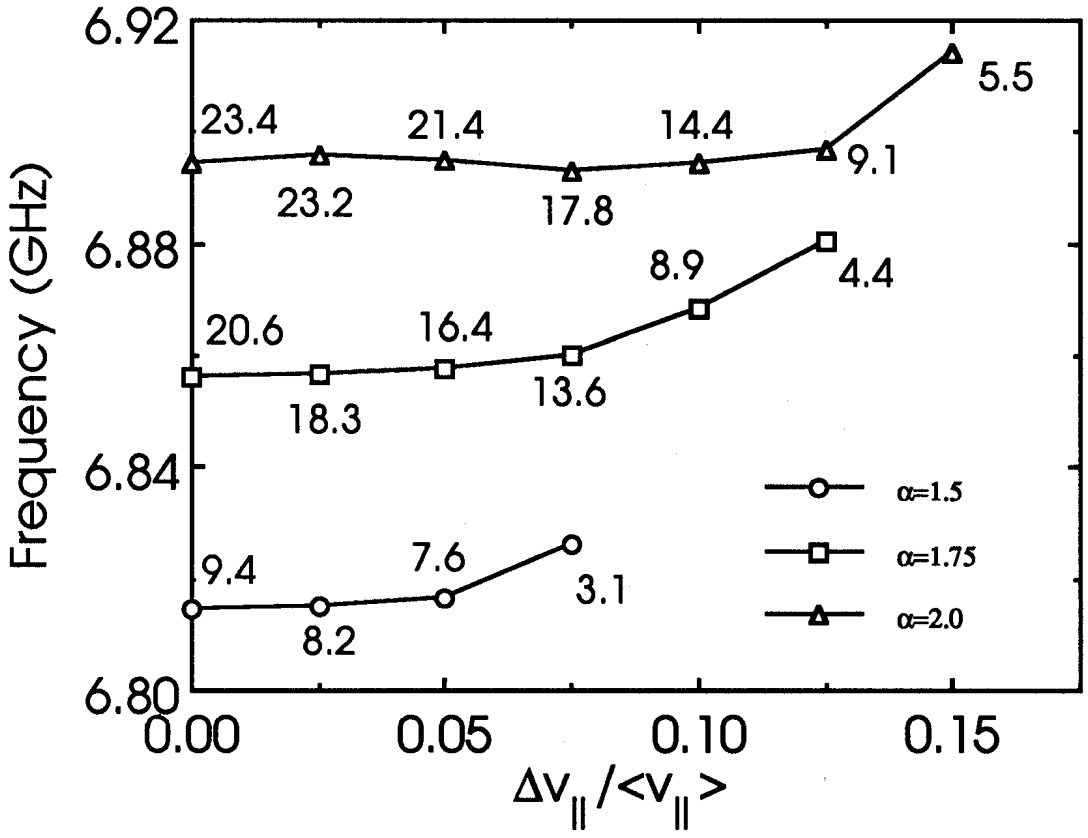

Figure 5

Computed oscillation frequency and output power (indicated in kW on the graph) of the TE_{21}^{o} gyro BW mode as a function of the parallel velocity dispersion $\Delta v_{||}/\langle v_{||}\rangle$. The low current density electron beam (j=2.7 A/cm^2, n_e=2.3·10^{15} electrons/m^3 at I_b=10 A) is characterized by $\Delta\gamma/\langle\gamma\rangle\cong 0$. The perpendicular velocity dispersion $\Delta v_{\perp}/\langle v_{\perp}\rangle$ corresponding to $\Delta v_{||}/\langle v_{||}\rangle$ is thus given by : $\frac{\Delta v_{\perp}}{\langle v_{\perp}\rangle} = \frac{1}{\alpha^2}\frac{\Delta v_{||}}{\langle v_{||}\rangle}$. U_{cath}=75 kV, I_b=4 A, B_0=2.97 kG and α=1.5 (circles), 1.75 (squares), 2.0 (triangles).

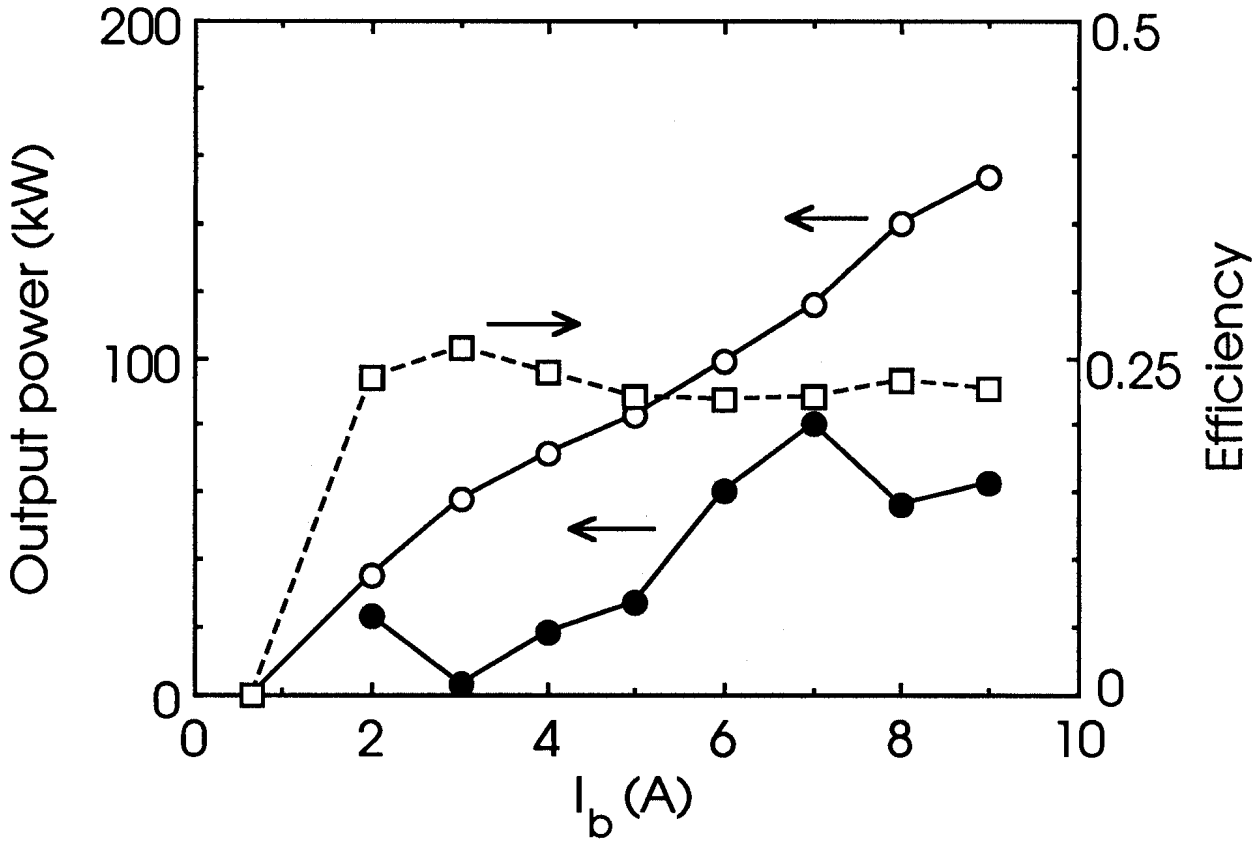

Figure 6

Results of the experimental optimization of the output power (open circles) and efficiency (open squares) of the TE^{o}_{011} mode. At each beam current I_b the oscillation of the TE^{o}_{21} gyro BW mode is observed at low power (P_{BW}<5 kW, filled circles = 20*P_{BW}) between 6.8 and 7.3 GHz, simultaneously with the TE^{o}_{011} gyrotron mode. U_{cath}=75 kV.

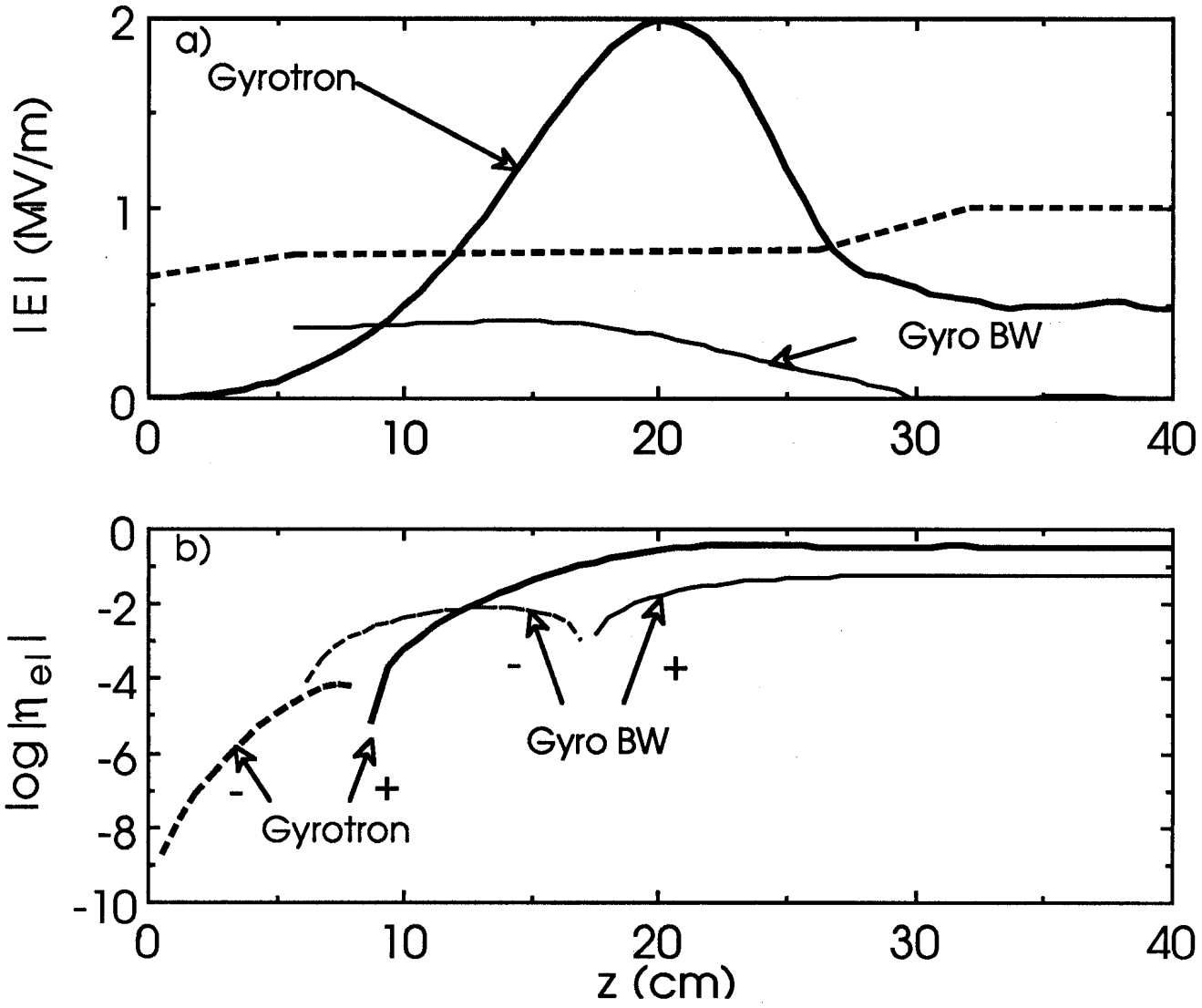

Figure 7

Computed single mode characteristics of the TE^{o}_{011} gyrotron and TE^{o}_{21} gyro BW modes along the cavity, for the same physical parameters : U_{cath}=75 kV, I_b=4 A, B_0=3.158 kG and α=1.75. a) Amplitude of the wave electric fields |E| (thick line : TE^{o}_{011} mode, thin line : TE^{o}_{21} mode) and cavity shape (dashed line, in a.u.). b) Logarithm of the absolute value of the electronic efficiencies η_{el}. The dashed lines correspond to the negative efficiencies in the region where particles absorb energy for their phase bunching (thick line mode TE^{o}_{011}, thin line mode TE^{o}_{21}).

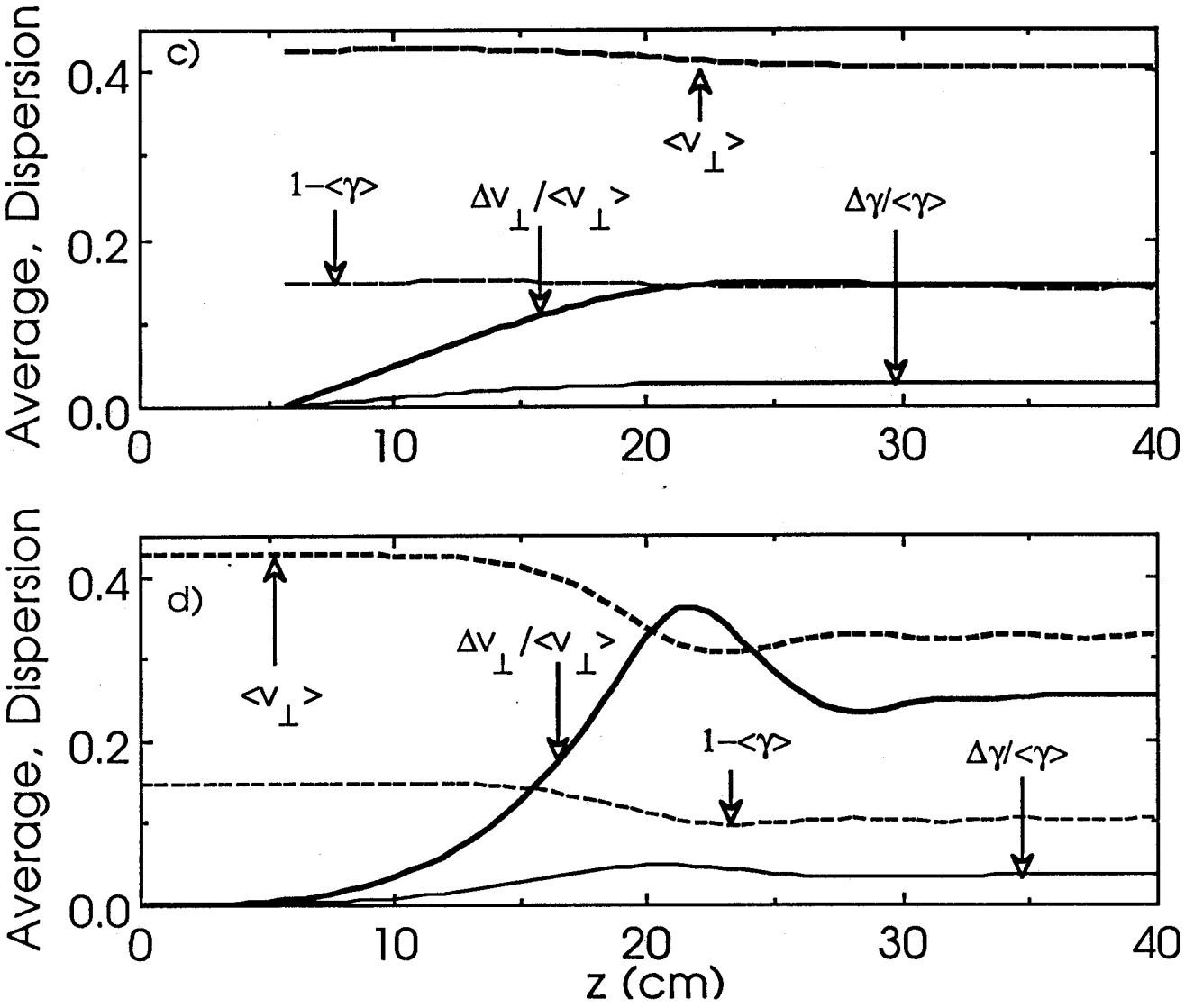

The dispersions ($\Delta v_\perp/\langle v_\perp\rangle$, $\Delta\gamma/\langle\gamma\rangle$) introduced by the oscillation of the two modes, together with the means values ($\langle v_\perp\rangle$, $1-\langle\gamma\rangle$), are plotted in figures c) and d) for the TE^{o}_{21} gyro BW and TE^{o}_{011} gyrotron modes, respectively. The two modes do not significantly change the parallel velocity ($\frac{\langle v_{||}\rangle_{out}}{v_{||0}}<0.01$, $\left.\frac{\Delta v_{||}}{\langle v_{||}\rangle}\right|_{out}<0.005$).

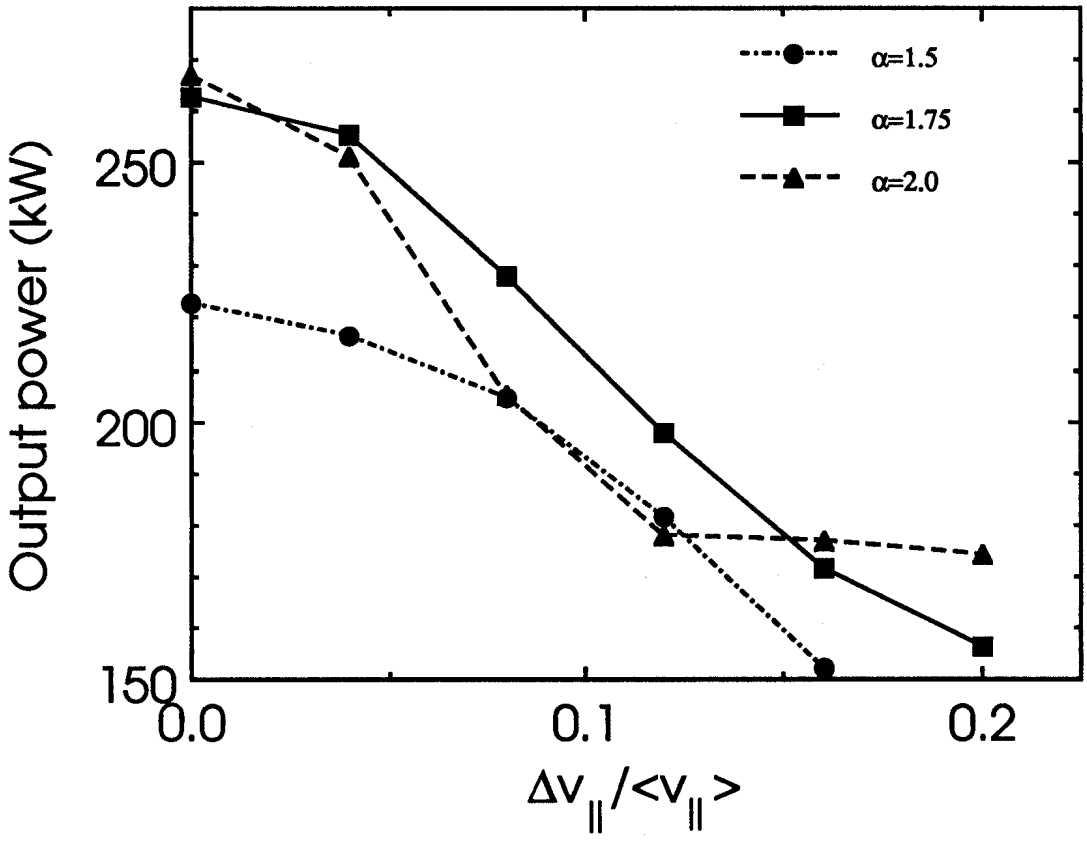

Figure 8

Effect of the velocity dispersion on the output power of the TE^{o}_{011} gyrotron mode. For the computation, a low charge density electron beam has been considered ($\Delta\gamma/\langle\gamma\rangle \cong 0$). The perpendicular velocity dispersion is thus related to the parallel one by : $\frac{\Delta v_{\perp}}{\langle v_{\perp}\rangle} = \frac{1}{\alpha^2}\frac{\Delta v_{\|}}{\langle v_{\|}\rangle}$. The velocity dispersions slightly decrease the oscillation frequency (-5 MHz for $\Delta v_{\|}/\langle v_{\|}\rangle = 0.2$ and $\alpha = 2.0$). Note that the output power obtained with $\alpha = 2.0$ is lower than with $\alpha = 1.75$ because the B-field is kept the same. It should be lowered to maximize the output power with $\alpha = 2.0$. $U_{cath} = 75$ kV, $I_b = 8$ A, $B_0 = 3.095$ kG, $\alpha = 1.5$ (circles), 1.75 (squares), 2.0 (triangles).

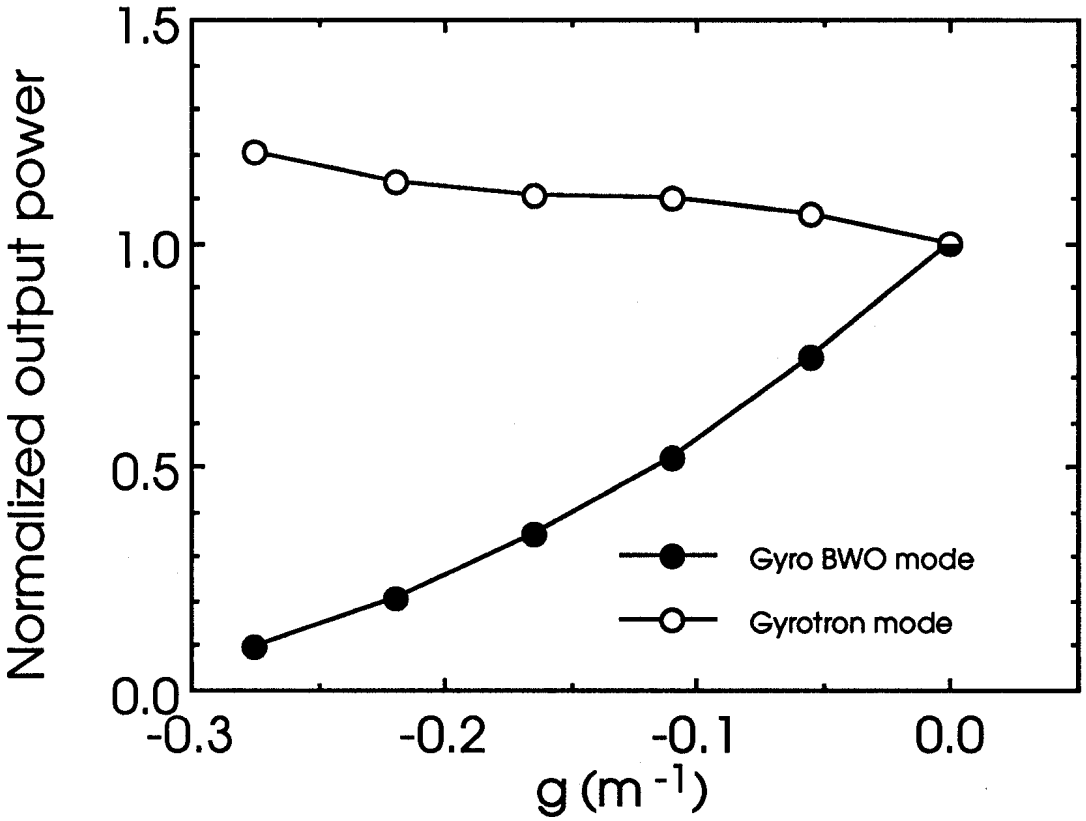

Figure 9

Influence of the negative B-field gradient ($g=\delta B_0/L_B B_0<0$) on the output power of the TE^{o}_{011} gyrotron mode (open circles) and of the TE^{o}_{21} gyro BW mode (filled circles), computed separately for the two modes (single mode calculation), but with the same physical parameters. The powers are normalized to their value with a flat B-field profile (g=0), 92.1 kW and 16.5 kW for the two modes, respectively. U_{cath}=75 kV, I_b=4 A, B_0=3.158 kG, α=1.75.

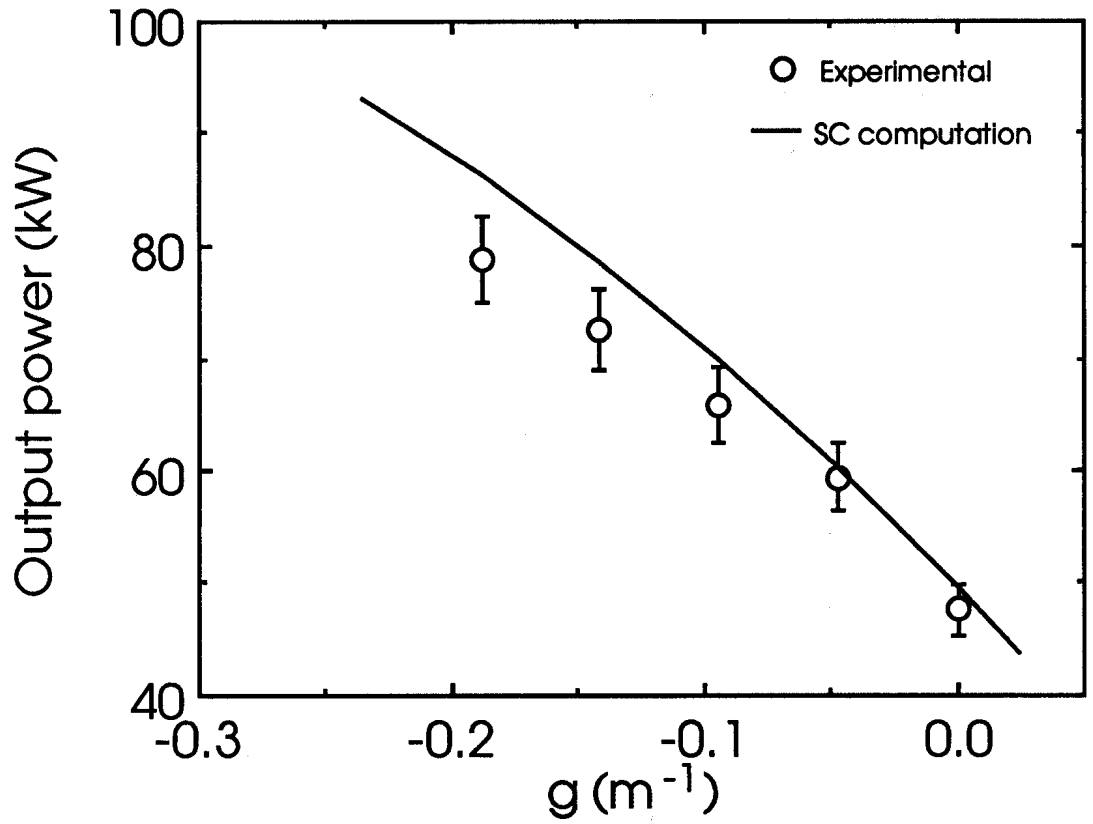

Figure 10

Comparison between the influence of the negative B-field gradient (g<0) on the output power of the TE^{o}_{011} gyrotron mode obtained experimentally (open circles) and computed self-consistently with the experimental values of α (α_{EGUN}) at the cavity input (continuous line). With g=0, the TE^{o}_{21} mode output power is very low (P_{BW}<0.2 kW) and has a little influence on the TE^{o}_{011} mode output power. The values of α are : α_{EGUN}= 1.50, 1.52, 1.68, 1.86, 2.35 for the respective values of g : g= 0.0, -0.047, -0.094, -0.141, -0.188. U_{cath}=75 kV, I_b=3 A, B_0=3.189 kG.

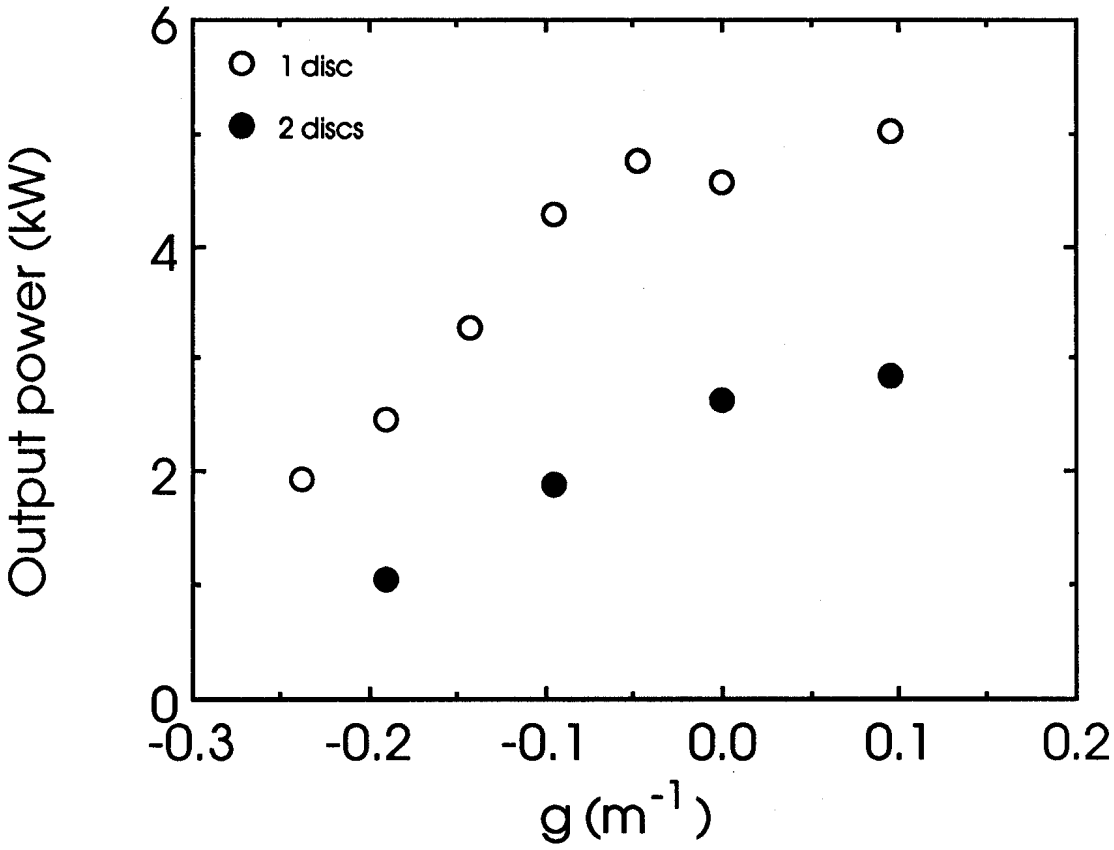

Figure 11

Influence of the B-field gradient $g=\delta B_0/L_B B_0$ on the output power of the TE^o_{21} gyro BW mode, measured at a B-field value where it oscillates in single mode, with a mismatched single disc alumina window (ρ=0.13-0.32 for the TE^o_{21} mode between 6.8 and 7.3 GHz, open circles) and with the matched window system (filled circles) consisting of two identical alumina discs separated by 3.9 cm (ρ=0.0-0.15). U_{cath}=75 kV, I_b=4 A, B_0=3.033 kG.

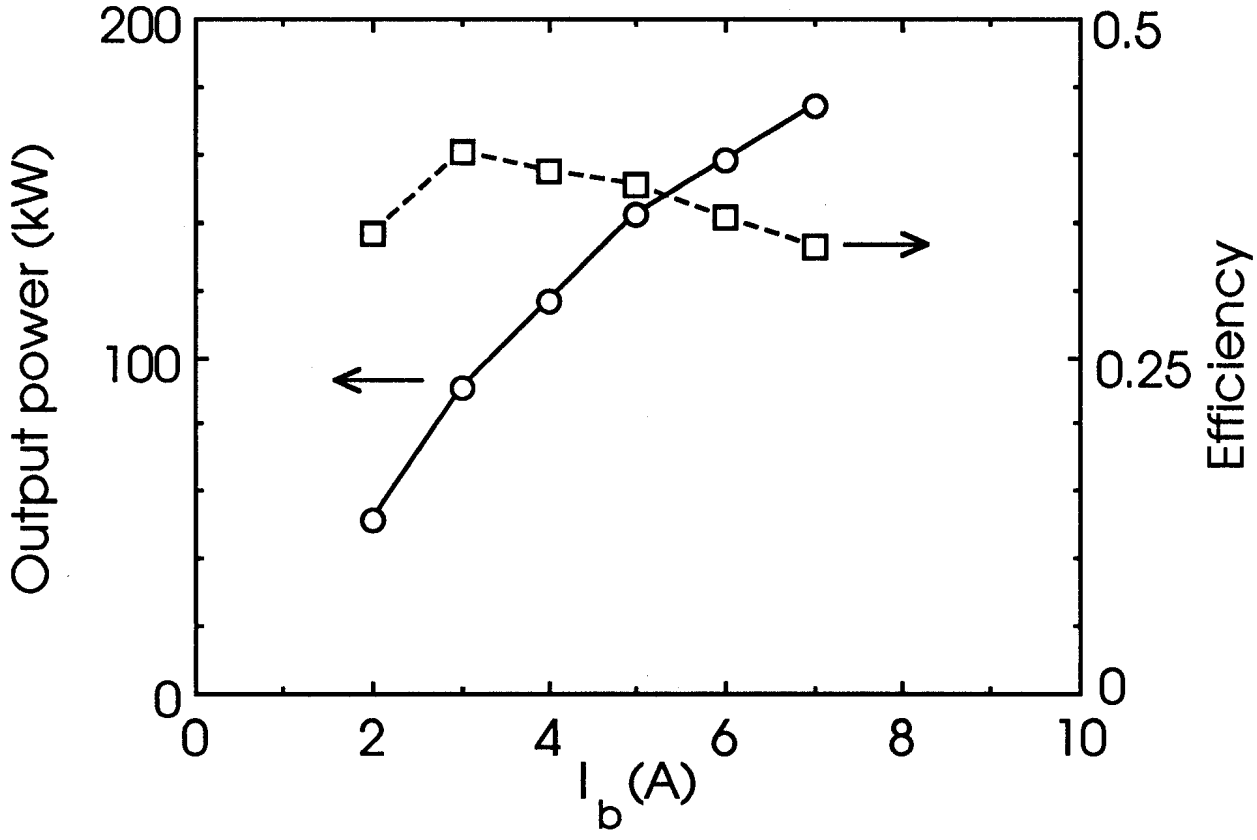

Figure 12

Results of the experimental optimization of the output power (circles) and efficiency (squares) of the TE^{o}_{011} mode with negative B-field gradient ($g<0$) along the electron beam to suppress the oscillation of the parasitic TE^{o}_{21} gyro BW mode. The output power and efficiency are multiplied by a factor 1.4 to 1.7 as compared with the results obtained with a flat magnetic field profile (cf. Fig. 6). U_{cath}=75 kV.

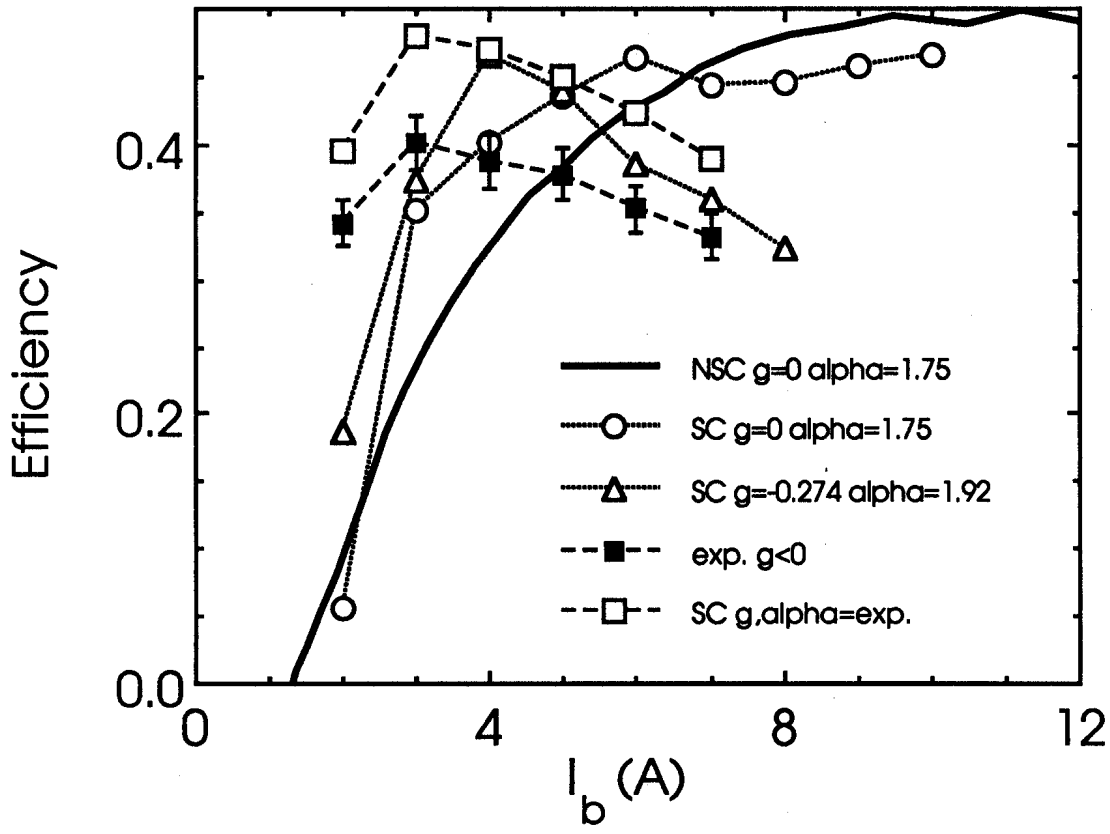

Figure 13

Efficiency computed non-self-consistently (thick continuous line) and self-consistently (open circles) for a flat B-field profile, with α=1.75, and computed self-consistently with a negative B-field gradient (g=-0.274) with α=1.92 (open triangles) at the cavity input. The value $\alpha(z=0)$=1.92 corresponds to α=1.75 at the middle of the cavity ($z=z_0$). The optimum experimental efficiency is obtained with the values α_{EGUN} given on Fig. 14 and with negative gradients B-field profiles (filled squares, -0.286<g<-0.143). The efficiency computed self-consistently with the experimental values of α and g (open squares) well reproduces the shape of the experimental result. U_{cath}=75 kV.

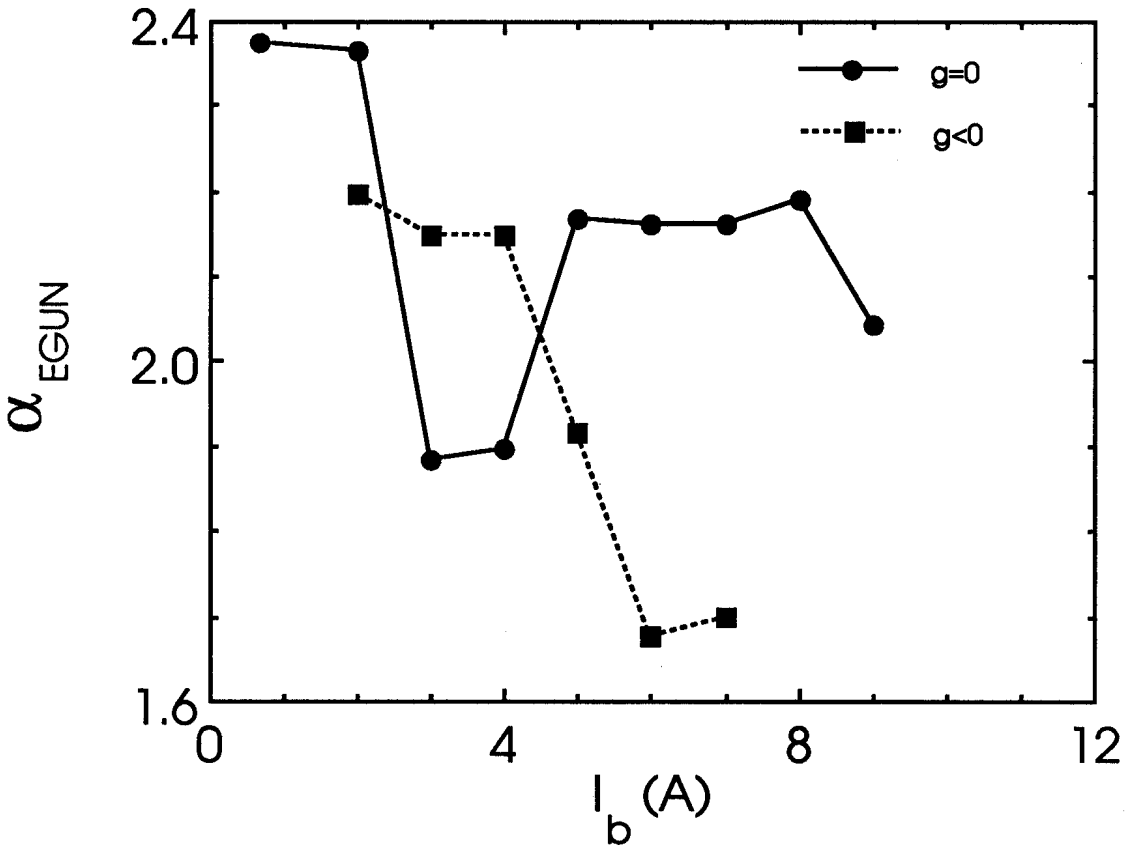

Figure 14

Values of $\alpha_{EGUN}=\langle v_\perp\rangle/\langle v_{||}\rangle$, as computed with the EGUN code from the experimental parameters for the output power optimization with a flat B-field profile (g=0, circles), corresponding to the results of Fig. 6, and with a negative gradient of the B-field profile along the electron beam flow (g<0, squares), corresponding to the results of Fig. 12. U_{cath}=75 kV.